HHS Public Access

Author manuscript

Neuroscience. Author manuscript; available in PMC 2017 December 17.

Published in final edited form as:

Neuroscience. 2016 December 17; 339: 85–99. doi:10.1016/j.neuroscience.2016.09.047.

Sex differences in astrocyte and microglia responses immediately following middle cerebral artery occlusion in adult mice

Helena W. Morrison, PhD[a,b] and **Jessica A. Filosa, PhD**[a]

Jessica A. Filosa: jfilosa@augusta.edu

[a]Augusta University, 1120 15th St, Augusta, GA 30912

Abstract

Epidemiological studies report that infarct size is decreased and stroke outcomes are improved in young females when compared to males. However, mechanistic insight is lacking. We posit that sex-specific differences in glial cell functions occurring immediately after ischemic stroke are a source of dichotomous outcomes. In this study we assessed astrocyte Ca^{2+} dynamics, aquaporin 4 (AQP4) polarity, S100β expression pattern, as well as, microglia morphology and phagocytic marker CD11b in male and female mice following 60 minutes of middle cerebral artery (MCA) occlusion. We reveal sex differences in the frequency of intracellular astrocyte Ca^{2+} elevations ($F_{(1,86)}$=8.19, *P*=0.005) and microglia volume ($F_{(1,40)}$=12.47, *P*=0.009) immediately following MCA occlusion in acute brain slices. Measured in fixed tissue, AQP4 polarity was disrupted ($F_{(5,86)}$=3.30, *P*=0.009) and the area of non-S100β immunoreactivity increased in ipsilateral brain regions after 60 min of MCA occlusion ($F_{(5,86)}$=4.72, *P*=0.007). However, astrocyte changes were robust in male mice when compared to females. Additional sex differences were discovered regarding microglia phagocytic receptor CD11b. In sham mice, constitutively high CD11b immunofluorescence was observed in females when compared to males (*P*=0.03). When compared to sham, only male mice exhibited an increase in CD11b immunoreactivity after MCA occlusion (*P*=0.006). We posit that a sex difference in the presence of constitutive CD11b has a role in determining male and female microglia phagocytic responses to ischemia. Taken together, these findings are critical to understanding potential sex differences in glial physiology as well as stroke pathobiology which are foundational for the development of future sex-specific stroke therapies.

Keywords

ischemic stroke; calcium; aquaporin 4; S100β; microglia morphology; CD11b

Correspondence to: Helena W. Morrison.

[b]Present address. University of Arizona, 1305 N. Martin Ave, P.O. Box 210203, Tucson, AZ 85721, hmorriso@email.arizona.edu

Disclosure

HWM contributed to the experimental design, execution of data collection, data analysis, data interpretation, and manuscript writing. JAF contributed to design of experiments, overall interpretation of data and manuscript editing. All authors read and approved the final manuscript.

The age-adjusted stroke mortality rate, which has been in decline since 2010, has been attributed to improved control of modifiable stroke risk factors such as hypertension, smoking, and dyslipidemia (Hoyert DL, 2012; Mozaffarian et al., 2015; Murphy et al., 2013). Yet In comparison, our understanding of a non-modifiable factors, such as sex differences, is lacking and therefore sex specific treatments are absent among stroke therapies. Emerging evidence taken from both epidemiological and pre-clinical stroke research supports the compelling assertion that sex has a dichotomous role in brain injury and functional outcomes after ischemic stroke (Go et al., 2014; Miller et al., 2011; Reeves et al., 2008). However, the diverging mechanisms of protection versus injury, which underlie this sexual dimorphism, have yet to be fully described and are not well understood (Banerjee et al., 2013; Ritzel et al., 2013).

Brain ischemia, caused by stroke, results in immediate neuronal death and the inevitable release of cell contents which then further disrupts finely tuned neuronal functions and promotes neuroinflammation (Dirnagl et al., 1999; Dirnagl, 2012; Gelderblom et al., 2009). Structurally, astrocytes are well positioned to intervene because of their intimate association with other glial cells, neurons, and blood vessels (Filosa et al., 2015). Functionally, astrocytes have a vital role in maintaining, mediating and restoring neuronal function during physiologic and pathologic conditions (Araque et al., 1999; del Zoppo, 2010; Nedergaard et al., 2010). In this role, astrocytes are key in maintaining K^+ homeostasis (Kofuji and Newman, 2004), removal of excess glutamate (Cheung et al., 2015), local blood flow regulation (Attwell et al., 2010; Kim et al., 2015), synaptogenesis and synaptic maintenance (Franke et al., 2012), among other functions. On the other hand, astrocyte dysfunction after ischemia may exacerbate brain injury via aberrant astrocyte Ca^{2+} signaling which can result in glutamate excitotoxicity (Nedergaard et al., 2010) or through the release of astrocyte-derived proteins and small molecular messengers such as ATP, TNFα, and S100β, which further increases neuroinflammation (Agulhon et al., 2012; Liu et al., 2011; Pascual et al., 2012). In addition, astrocyte aquaporin 4 (AQP4) is a water channel and key player in the development of brain edema. AQP4 is primarily localized to astrocyte endfeet rather than non-endfeet processes and this polarized location has an important role in brain fluid clearance (Gaberel et al., 2014; Iliff et al., 2013). AQP4 polarity is disrupted in the days following traumatic brain injury (Kress et al., 2014; Plog et al., 2015) and transient focal ischemia (Fukuda and Badaut, 2012; Vella et al., 2015) which may contribute to brain edema after injury. Importantly, brain edema is accompanied by increased astrocyte intracellular Ca^{2+} (Thrane et al., 2011). However, it is yet unknown if changes in astrocyte Ca^{2+} dynamics, the expression pattern of S100β and AQP4 polarity is altered immediately following middle cerebral artery (MCA) occlusion in adult male and female mice.

Adding to the complexity of cell-to-cell interactions, microglia are phagocytes and, in conjunction with astrocytes, contribute to the inflammatory milieu after ischemic stroke. Microglia cells are highly sensitive to altered brain physiology because of their constant monitoring and immediate inflammatory response to pathophysiology (i.e. ischemia). These important functions are made possible by their ramified morphology (Morrison and Filosa, 2013), dynamic process movement (Davalos et al., 2005), consistent distribution throughout the brain (Lawson et al., 1990), and continuous input from neurons and astrocytes via small

molecular messengers (i.e. fractalkine and S100β respectively) (Bianchi et al., 2010; Madry and Attwell, 2015). We previously reported that microglia morphology and phagocytic receptor CD11b are immediately changed by brain ischemia and therefore can be used as an indicator of an early microglia response to stroke (Morrison and Filosa, 2013). However, sex differences in microglia responses to ischemia are largely unknown. Microglia phagocytosis, initiated in part by CD11b-ligand interactions, is a double-edged sword; necessary for wound healing but also well documented in pre-clinical research as a source of secondary inflammatory injury after stroke (Brown and Neher, 2012; Lee et al., 2014). Understanding this balance in both males and females is relevant to future stroke therapies which are developed to promote brain recovery and yet must also account for inherent secondary injury.

Unfortunately, few pre-clinical stroke-related studies have examined glial (astrocyte and microglia) responses to injury in male and female adult mouse models prior to 24 hours post-ischemia (Cordeau et al., 2008). As a result, our understandings of early glial events that may be central brain injury after ischemic stroke are only beginning to be revealed (Zheng et al., 2010; Zheng et al., 2013). Moreover, it is not clear if early astrocyte and microglia responses to ischemia are different between male and female mice. Such information is vital in establishing a timeline of sex differences after ischemic stroke and therefore vital to the discovery and implementation of potential sex-specific stroke treatment regimens. In this study, we determine sex differences in astrocyte and microglia responses to 60 min of MCA occlusion in adult male and female mice by assessing changes in astrocyte Ca^{2+} dynamics and microglia volume in acute brain slices. In addition, we illustrate sex differences in astrocyte S100β and AQP4 immunofluorescence patterns as well as microglia CD11b immunoreactivity after 60 min of MCA occlusion.

1.1 Experimental Procedures

Animals

Male $CX_3CR_1^{GFP/GFP}$ mice with a C57BL6/J background (Jackson Laboratories, no. 005582) were bred to female C56BL6/J mice. Heterozygous male and female offspring $CX_3CR_1^{GFP/+}$ weighing 20–25 g (6–8 weeks old) were used to record somatic astrocyte Ca^{2+} elevations and microglia volume after ischemia and in acute brain slices. For consistency, $CX_3CR_1^{GFP/+}$ mice were used for additional immunohistochemistry (IHC) experiments. All animals were housed in climate controlled rooms with a 12-h light cycle. Female mice were not subjected to estrous cycle synchronization, but were allowed to cycle naturally. Female mice were sampled randomly to determine if ischemia induced astrocyte and microglia responses were present despite possible variations in sex hormone levels, an occurrence that more accurately models the human condition and an appropriate initial inquiry (McCarthy et al., 2012). All animal experiments were performed according to methods approved by and in compliance with the Augusta University Institutional Animal Care and Use Committee.

Middle cerebral artery occlusion

Focal cerebral ischemia to the right hemisphere was achieved using the filament method to occlude the right MCA for 60 min in male and female animals under isoflurane anesthesia delivered via a 20% oxygen/80% air mixture as previously described (Morrison and Filosa, 2013). After common, internal and external artery dissection, a heat blunted and silicone-coated filament (tip diameter 0.20–0.25 mm) was advanced to the ostea of the MCA through the external and internal common carotid artery. Cerebral ischemia to the right MCA region was verified by laser Doppler flowmetry (Perimed Periflux 5000, North Royalton, OH); animals were included in the study if ischemia resulted in a > 70% reduction in blood flow. Focal ischemia was maintained for 60 min. The sham procedure included all elements up to filament placement. All animals were euthanized without reperfusion and prior to brain tissue collection for acute brain slices or tissue processing for IHC methods.

Acute brain slices and brain cell imaging

Acute brain slices were acquired for *ex vivo* astrocyte and microglia imaging in a group of naïve animals (no surgery) or immediately after 60 min MCA occlusion. Brain tissue was extracted immediately after euthanasia in ice-cold artificial cerebral spinal fluid (aCSF) and immediately sliced into 280 μm coronal sections using a vibratome as previously described (Leica VT 1200S, Leica Microsystems, Wetzlar, Germany)(Morrison and Filosa, 2013). The composition of aCSF was (in nM): KCl 3, NaCl 120, $MgCl_2$ 1, $NaHCO_3$ 26, NaH_2PO_4 1.25, glucose 10, $CaCl_2$ 2 and 400 μM L-ascorbic acid; osmolarity was 300–305 mOsM and pH to 7.4 after 95% O_2 and 5% CO_2 equilibration. Brain hemisphere sections (no surgery, contralateral and ipsilateral) were incubated in aCSF containing the Ca^{2+} indicator Rhod-2AM (Molecular Probes, MP 01244, 5μM) and 2.5 μL 20% pluronic acid (Molecular Probes P3000MP) in a 95% O_2/5% CO_2 oxygenated chamber for 60 min just prior to imaging. Figure 1A summarizes the experimental protocol for Ca^{2+} imaging after 60 min MCA occlusion.

Astrocyte Ca^{2+} imaging—All images were acquired in cortical layers I–III using a 40× objective (Zeiss Achroplan 40×/0.8w) at a rate of 4 images per second. To test astrocyte viability, ATP (Sigma, A 9187, 500 μM) was bath applied at the end of each experiment; only astrocytes responsive to ATP, determined by a robust increase in intracellular Ca^{2+}, were included in the data analysis. Live imaging was limited to a 3 hour window following incubation with the Ca^{2+} indicator. Calcium imaging was analyzed as previously described using Sparkan software [Dr. Adrian Bonev, University of Vermont (Filosa et al., 2004)]. Fluorescence intensity (F) was determined within 10 × 10 pixel squares placed over Rhod-2 loaded astrocytes with baseline fluorescence (F_0) determined from 20 images showing no activity. Fractional fluorescence (F/F_0) was calculated and peaks were automatically detected from oscillations crossing a set threshold value (>0.2 F/F_0) and summarized as Ca^{2+} oscillations peak frequency (Hz) for each cell. We quantified the area under the curve (AUC) of each Ca^{2+} trace as an additional indicator of astrocyte Ca^{2+} which accounts for both peak frequency, amplitude and duration. Using the same 10 × 10 pixel region of interest, AUC was calculated as the integral over time for each cell exhibiting Ca^{2+} activity included in the study (Kim et al., 2015). All data was normalized to appropriate male and female naïve/no surgery group for statistical analysis.

Microglia imaging—$CX_3CR_1^{GFP/+}$ microglia adjacent to astrocytes were imaged immediately following astrocyte Ca^{2+} imaging. We imaged microglia soma and associated processes by acquiring Z-stack confocal images every 1 μm for 30–35 μm to ensure that we included the same imaging plane used for astrocyte Ca^{2+} acquisition. IMARIS software (Bitplane) and filament building protocols were used to create representative 3D microglia models, necessary to quantify the volume of each microglia. Data were normalized to appropriate male and female naïve/no surgery group prior to two-way statistical analysis.

Immunohistochemistry

Immunohistochemistry (IHC) images were acquired in additional male and female groups of mice. After 60 min MCA occlusion or sham surgery, animals were euthanized, brain tissue removed, fixed for 24h in 4% paraformaldehyde and incubated in a 30% sucrose solution for 72h. Brain tissue was kept at −80°C until sectioning into coronal sections (Leica cryostat CM3050, 50μm) and stored at −20°C in a cryoprotectant solution until tissue processing for IHC staining. To identify astrocytes and microglia, free-floating brain sections were blocked in a 10% horse serum solution (0.01M PBS 0.05% Triton and 0.04% NaN_3) for 1h followed by a 72h incubation with primary antibodies: rabbit anti-GFP 1:1,000 (Invitrogen A-6455), rat anti-Mac-1 1:500 (Chemicon MAB1387Z), rabbit anti-S100β 1:200 (Dako Z031101-2), and goat anti-AQP4 1:500 (Santa Cruz sc-9888). A 4-h incubation of 1:250 secondary primaries followed: donkey anti-rabbit Alexa 488, (711-546-152); donkey anti-rat CY3, (712-166-153); donkey anti-chicken Alexa 649 (702-605-155) and donkey anti-goat 594, (705-585-147, Jackson ImmunoResearch Laboratories). Our IHC protocol was for double staining of anti- AQP4 and anti-S100β in one set of male and female tissue and, in another set of tissue, double staining of anti-GFP and anti-CD11b. Male and female tissues from sham and ischemic groups were incubated together for consistent IHC staining. In addition, sections of ipsilateral proximal female brain tissue that was subjected to all aspects of our ICH protocol but without primary antibody. This secondary only antibody staining assessed unspecific binding that may have been prevalent in the infarcted area. All reactions were carried forward at room temperature; washes between incubations were done with 0.01M PBS for 15min. Slices were then mounted onto slides using Vectashield (Vector Laboratories, H-1000).

Image acquisition and analysis

A confocal microscope was used to acquire photomicrographs (30-μm Z-stack at 2-μm intervals, Zeiss 510, 40×/1.3 oil objective) of cortical layers I–III after IHC preparation in brain regions depicted in Figure 3A. Photomicrographs were stacked and split to obtain maximum intensity projections for all channels and saved as TIFF files prior to analysis. The location of astrocyte AQP4 and S100β was determined as well as microglia morphology and CD11b after 60 min MCA occlusion in male and female tissue.

Astrocyte S100β analysis—With injury, S100β is released in macro-molar concentrations from the astrocyte soma to the extracellular space. We determined changes in S100β location, from primarily somatic to non-somatic areas, after 60min MCA occlusion and tested if post-stroke changes were different between male and female mice. The distribution pattern of S100β was determined from photomicrographs with a three step

analysis technique using Image J software (http://imagej.net). The S100β analysis technique was derived from previous studies examining changes in the area of AQP4 distribution [(Ren et al., 2013; Wang et al., 2012) described below]. For each photomicrograph, we first we determined the area of S100β positive immunofluorescence which included both somatic and non-somatic S100β immunoreactivity (Figure 3B low threshold). Second, we determined the area of S100β positive immunofluorescence that included primarily somatic S100β immunofluorescence (Figure 3B high threshold). Third, the area of non-somatic S100β was calculated: (area of somatic and non-somatic S100β immunoreactivity) − (area of somatic S100β immunoreactivity) = area of non-somatic immunoreactivity. An example of this process is illustrated in Figure 3B.

Astrocyte AQP4 analysis—In astrocytes, the water channel AQP4 is constitutively expressed and polarized to astrocyte endfeet rather than astrocyte soma or other processes. AQP4 polarity is disturbed with brain injury and this change in AQP4 distribution (from endfeet to non-endfeet locations) has been previously quantified using IHC photomicrographs and image analysis (Ren et al., 2013; Wang et al., 2012). We employ this method by first determining the area of AQP4 immunoreactivity at astrocyte endfeet as well as in non-endfeet astrocyte processes (Figure 4A low threshold). Second, we determined the area of AQP4 immunoreactivity in astrocyte endfeet (Figure 4A high threshold). AQP4 polarity was calculated: (area of endfeet and non-endfeet AQP4 immunoreactivity) − (area of endfeet AQP4 immunoreactivity) = un-polarized AQP4 immunoreactivity. An example of this process is illustrated in Figure 4A.

Microglia analysis—Microglia were analyzed for changes in morphology and phagocytic function using a computer-aided skeleton analysis method (microglia processes length and number of endpoints) and CD11b immunofluorescence, respectively, as previously described (Morrison and Filosa, 2013). For computer-aided morphological analysis, anti-GFP images were despeckled and then processed to create skeletonized images using Image J software. The Analyze Skeleton Plugin (Arganda-Carreras et al., 2010) was used to identify (tag) and microglia skeletons relevant to quantify ramification: slab voxels, junctions and endpoints. Figure 5B illustrates the conversion from despeckled to tagged image. We summarized the number of endpoints and averaged the length of all processes (slab voxels) from the Analyze Skeleton plugin data output. We then normalized all data by the number of somas/image to result in number of endpoints/cell and microglia process length/cell. Microglia CD11b total fluorescence intensity (TFI) was determined in male and female tissue as previously published. Briefly, microglia CD11b TFI was determined by multiplying the percent area of the image with positive immunoreactivity by the mean fluorescence intensity of CD11b immunoreactivity.

Statistical Analysis

Sex differences in control conditions (no surgery and sham groups) were determined using Student’s t-test. Data collected after 60min MCA occlusion were normalized to male or female no surgery or sham conditions and two-way ANOVA was then used to test for sex differences and brain regions affected by the MCA occlusion. Sidak’s multiple comparisons

post-hoc test was used to test for specific differences between groups. All data are presented as the mean ± standard error of mean (SEM). GraphPad Prism 6 was used for all analyses.

1.2 Results

Sex differences in astrocyte Ca^{2+} elevations after 60 min MCA occlusion

We examined the effect of MCA occlusion on astrocyte Ca^{2+} dynamics in cortical brain regions immediately following 60 min MCA occlusion in adult male and female acute brain slices. A summarized protocol and brain regions (contralateral, ipsilateral distal and ipsilateral proximal) for astrocyte Ca^{2+} imaging are shown in Figure 1A. Representative astrocyte Ca^{2+} traces used to analyze AUC and peak frequency (Hz) are shown in Figure 1B. There were no sex differences in astrocyte Ca^{2+} AUC between male and female no surgery groups (Figure 1C, **left**). Data summarized by Figure 1C (right) was normalized to the no surgery group in each sex to determine changes in astrocyte AUC in brain regions affected by the MCA occlusion. There was no significant region or sex effect observed for Ca^{2+} AUC after 60min MCA occlusion (Two-way ANOVA: region $F_{(3,72)}=0.20$, $p = 0.9$, sex: $F_{(1,72)}=2.639$, $p=0.11$, interaction $F_{(3,72)}=0.50$, $p=0.68$). We also summarized astrocyte Ca^{2+} peak frequency from astrocyte Ca^{2+} traces; there were no sex differences in astrocyte Ca^{2+} peak frequency between male and female no surgery groups (Figure 1D, **left**). Data summarized by Figure 1D (right) was normalized to the no surgery group in each sex to determine changes in the frequency of astrocyte Ca^{2+} elevations in brain regions affected by the MCA occlusion. A two-way ANOVA analysis reveals sex differences in Ca^{2+} peak frequency after ischemia but astrocyte Ca^{2+} peak frequency was not significantly different between brain regions (Figure 1D; region $F_{(3,86)}=0.25$, $p=0.86$, sex: $F_{(1,86)}=8.19$, $p=0.005$, interaction $F_{(3,86)}=1.75$, $p=0.16$). Post-hoc testing of sex differences revealed that astrocyte Ca^{2+} peak frequency was increased in female ipsilateral tissue when compared to males.

Sex differences in microglia volume resulting from 60 min MCA occlusion

We imaged microglia from male and female $CX_3CR_1^{GFP/+}$ mice subjected to 60 minutes MCA occlusion in mice in order to quantify changes in microglia volume. Microglia volume was calculated from 3D models generated using IMARIS (Bitplane) filament tracer protocols. A representative image of a microglia in each region (no surgery, contralateral, ipsilateral distal and ipsilateral proximal) and its corresponding IMARIS model used to determine volume is shown in Figure 2A. There were no sex differences in microglia volume between male and female no surgery groups (Figure 2B, **left**). Microglia volume data was normalized to male or female no surgery group in order to determine changes in volume affected by the MCA occlusion and summary data are shown in Figure 2B (right). Microglia volume was not significantly changed in brain regions after MCA occlusion but was different between male and female mouse groups after ischemia (two-way ANOVA: region $F_{(3,40)}=11.87$, $p<0.08$, sex: $F_{(1,40)}=12.47$, $p=0.009$, interaction $F_{(3,4)}=8.80$, $p=0.17$). Post-testing of sex differences revealed no specific differences in microglia volume in the ipsilateral hemisphere after MCA occlusion.

Sex differences in S100β expression pattern after 60 minutes of MCA occlusion

The Ca^{2+} binding protein S100β is typically expressed in astrocyte soma, its release is a biomarker of brain injury (Dayon et al., 2011; Plog et al., 2015). Figure 3A illustrates the representative brain regions for data collection in proximity to the ischemic injury (contralateral, distal ipsilateral and ipsilateral proximal region); matching regions were acquired in sham tissue. The protocol used to measure non-somatic S100β expression, described in Methods, is illustrated in Figure 3B. Exemplar photomicrographs used for image analysis and data collection are shown in Figure 3C. Cropped images, shown below the full sized photomicrographs, illustrate the details of S100β immunofluorescence and changes to the expression pattern after MCA occlusion in male and female animals. We determined the change in S100β expression pattern after 60 min ischemic stroke in male and female mice using uncropped photomicrographs. Unspecific secondary binding of anti-rabbit 594 to the ipsilateral proximal region was not detectable. There were also no sex differences in the area of non-somatic S100β between male and female sham groups (Figure 3D, **left**). S100β data were normalized to the male or female sham group in order to determine changes in the area of S100β immunoreactivity after MCA occlusion according to sex and brain regions (Figure 3D, **right**). Significant effects were noted for both region and sex (two-way ANOVA: region: $F_{(5,86)}=4.72$, $p=0.007$, sex: $F_{(1,86)}=10.25$, $p=0.0019$, interaction $F_{(5,86)}=1.81$, $p=0.12$). Post-hoc testing revealed that in the male, but not female, non-somatic S100β immunoreactivity was robustly increased after MCA occlusion in the proximal ipsilateral region when compared to sham and contralateral regions.

Sex differences in AQP4 polarity after 60 minutes of MCA occlusion

Changes in AQP4 expression are well documented in ischemic stroke (Ribeiro Mde et al., 2006; Vella et al., 2015; Wang et al., 2012). However, the expression pattern in male and female brain tissue has not been previously addressed. The protocol used to measure un-polarized AQP4 expression, described in Methods, is illustrated in Figure 4A. Examples of IHC-AQP4 images used for our image analysis protocol are shown in Figure 4B with cropped photomicrographs shown below to better illustrate changes in the AQP4 expression pattern. Unspecific secondary binding of anti-goat 647 to the ipsilateral proximal region was not detectable. In sham mice, sex differences exist in AQP4 polarity (Figure 4C, **left**). However, this change in AQP4 polarity was only observed in the proximal region (Student's t-test, $p = 0.05$). AQP4 data were normalized to male or female sham group in order to determine changes in AQP4 polarity after MCA occlusion according to sex and brain regions (Figure 4C, **right**). Changes to AQP4 polarity was significantly changed in brain regions and according to sex after 60 min MCA occlusion (two-way ANOVA: region $F_{(5,86)}=3.30$, $p=0.009$, sex: $F_{(1,86)}=17.21$, $p<0.0001$, interaction $F_{(5,86)}=2.17$, $p=0.06$). Post-hoc testing reveals significant changes in AQP4 polarity in ipsilateral brain regions after MCA occlusion in male and not female mice. Sex differences exist in AQP4 polarity in distal contralateral and ipsilateral brain regions.

Sex differences in microglia morphology after 60 min MCA occlusion

We investigated sex differences in microglia neuroinflammatory responses to ischemia in addition to astrocyte responses. We first quantified microglia morphology after 60 min MCA

occlusion in male and female mice in sham, contralateral and ipsilateral (proximal and distal) regions as shown in Figure 3A. Cropped single cells from photomicrographs are included to better visualize microglia morphology details; data analysis was conducted on uncropped images. Microglia morphology (number of microglia process endpoints/cell and process length/cell) was determined from anti-GFP photomicrographs using a skeleton analysis method that was modified from our previous publication (Morrison and Filosa, 2013) and summarized in Figure 5B. As expected, unspecific secondary binding (anti rabbit 488) to the ipsilateral proximal region was not detected, however, faint GFP fluorescence of microglia in the $CX_3CR_1^{GFP/+}$ mouse was present, not shown. There were no sex differences in microglia process length/cell or endpoints/cell between male and female sham groups (Figure 3D **left and** Figure 4D **left**, respectively). Microglia morphology data were normalized to male or female sham group in order to determine changes after MCA occlusion according to sex and brain regions; summary graphs of these normalized data are shown in Figure 5D and Figure 5E. Our analysis reveals that microglia process endpoints/cell were different after MCA occlusion according to region and sex (two-way ANOVA: region $F_{(5,86)}=4.74$, $p = 0.0007$, sex: $F_{(1,86)}=18.29$, $p < 0.0001$, interaction $F_{(5,86)}=4.74$, $p = 0.0007$). However, a significant interaction effect, observed here, indicates that the two factors sex and ischemia are interdependent. On the other hand, microglia process length/cell after MCA occlusion was not altered by either sex or region (Figure 5D; two-way ANOVA: region $F_{(5,86)}=1.93$, $p=0.10$, sex: $F_{(1,86)}=1.04$, $p=0.31$, interaction $F_{(5,86)}=0.49$, $p=0.78$).

Sex differences in microglia CD11b in sham mice and after 60 min MCA occlusion

In addition to morphology, we examined microglia function after 60 min MCA occlusion; microglia CD11b is an important receptor to microglia phagocytosis. Example images in all male and female tissue after sham and MCA occlusion are shown in Figure 6A. Cropped single cells from photomicrographs are included to better visualize CD11b immunofluorescence. The CD11b receptor is located on cell processes as well as, to a lesser extent, on the soma (Perego et al., 2011) which we show in Figure 6B (anti-GFP shows microglia (top) with matching anti-CD11b immunofluorescence below). Unspecific secondary binding of anti-rat CY3 secondary to the ipsilateral proximal region was not detectable. Typically, the intensity of CD11b immunoreactivity is increased in response to injury (Morrison and Filosa, 2013; Perego et al., 2011). However, we show that microglia CD11b immunofluorescence staining is prevalent in female sham tissue when compared to male sham tissue (Figure 6C; Student's t-test: $p = 0.03$). In addition to these baseline sex differences, we also observed sex differences in microglia CD11b immunofluorescence after 60 min MCA occlusion. For this analysis, CD11b data was normalized to male or female sham group in order to determine changes after MCA occlusion according to sex and brain regions; summary graphs of these normalized data are shown in Figure 6D (two-way ANOVA: region $F_{(5,86)}=8.74$, $p=0.07$, sex: $F_{(1,86)}=13.12$, $p=0.0001$, interaction $F_{(5,86)}=7.44$, $p=0.11$). Post-hoc testing reveal that changes to microglia CD11b is robust after 60 min of MCA occlusion in male proximal brain regions but absent in the female tissue. To summarize: 1) constitutive CD11b immunofluorescence is greater in females than males; 2) in female mice, constitutively high CD11b remains unchanged after 60 min MCA occlusion whereas, 3) in male mice, constitutively low CD11b is robustly increased in proximal ipsilateral regions after 60 min of MCA occlusion.

1.3 Discussion

We provide evidence of sex differences in the frequency of astrocyte Ca^{2+} elevations and microglia volume after 60 min MCA occlusion which was measured in acute brain slices. Using IHC methods, we show that astrocytes and microglia have a robust immediate response to MCA occlusion that is sex dependent. Significant changes in the ipsilateral hemisphere immediately after MCA occlusion included: increased presence of non-somatic S100β; un-polarized AQP4; and higher microglia CD11b immunofluorescence in male but not female mice. In addition, the prevalence of microglia CD11b immunofluorescence at baseline in females, when compared to males, brings to light sex differences in constitutive microglia function which, we suggest, may have a role in determining male and female microglia responses to ischemia.

Detrimental neuronal cortical spreading depolarizations and glutamate excitotoxicity, hypothesized to occur in the peri-infarct region following ischemia (Hinzman et al., 2015), stands as an early injurious event following stroke as well as a mechanism of delayed neuronal cell death (Dirnagl et al., 1999). Increased astrocyte Ca^{2+} elevations, mediated in part by neuronal release of glutamate (Kim et al., 1994), also contributes to edema (Thrane et al., 2011) and the neurotoxic events after ischemia (Ding et al., 2009; Hansson and Ronnback, 2003; Iwabuchi and Kawahara, 2009; Nedergaard and Dirnagl, 2005; Takano et al., 2009). We did not observe sex differences between our control (no surgery) groups and therefore baseline conditions did not have an effect on our post-ischemia analysis. Out data suggest that changes in the frequency of astrocyte Ca^{2+} elevations were small in the ipsilateral brain regions after 60 min of MCA occlusion in both male and female mice. Our findings differ from Ding and colleagues (2009) who revealed robust and sustained increases in astrocyte Ca^{2+} elevations measured in male mice using a photothrombotic stroke *in vivo* model (Ding et al., 2009). Methodological factors could account for observed differences between studies. For example, the bulk loading of Ca^{2+} indicators, a method used in this study, limits data collection to the cell soma and excludes detection of astrocyte Ca^{2+} responses in processes (Bazargani and Attwell, 2016). Therefore, our data may under-represent astrocyte Ca^{2+} dynamics after ischemic stroke (Srinivasan et al., 2015). Also possible, the focal ischemic injury from the filament method and MCA occlusion may not have provided sufficient cortical injury for a robust astrocyte Ca^{2+} response in the ipsilateral hemisphere. Methodologic constrains limited our ability to directly measure brain cell injury concurrent to *ex vivo* astrocyte imaging. In lieu, we measured microglia volume as an indirect indicator of cell injury. We show that microglia volume in control groups were similar and were not significantly changed after MCA occlusion in either male or female mice which suggests that brain injury was mild at this early time point.

Similar to microglia volume, we did not observe sex differences in astrocyte Ca^{2+} elevations at baseline. However, we observed sex differences in astrocyte Ca^{2+} elevations after 60 min MCA occlusion. The frequency of astrocyte Ca^{2+} elevations in the ipsilateral hemisphere was increased in females when compared to males. It is possible that estradiol has a role in increasing astrocyte Ca^{2+} dynamics in female mice. In cell culture models, estradiol is shown to promote signaling mechanisms that increase intracellular Ca^{2+} concentrations and corresponding astrocyte Ca^{2+} dependent functions (Chaban et al., 2004; Kelly and

Ronnekleiv, 2009). While not tested in our preparation, estradiol was reported to increase cytoplasmic Ca^{2+} release in cultured hypothalamic astrocytes collected from both males and females but not in females with estrogen receptor knockout (Kuo et al., 2010). It has also been shown that elevated intracellular Ca^{2+} stimulates astrocyte mitochondrial metabolism to maintain vital energy resources during the first few hours after ischemia. In this case, increased intracellular Ca^{2+} is associated with markedly improved post-stroke neurological outcomes (Zheng et al., 2010; Zheng et al., 2013). Taken together our data supports increased frequency of astrocyte Ca^{2+} elevation as a mechanism driving dichotomous stroke outcomes between males and females. However, it remains that our understanding of sex differences on constitutive or injury-evoked astrocyte Ca^{2+} dynamics in adult mice and resulting influence on brain function remains incomplete and is an area of study that warrants additional investigation.

In addition to measuring astrocyte Ca^{2+} dynamics, we investigated the potential of sex differences in the location of astrocyte AQP4 and S100β, proteins suspected to play a role in brain injury after ischemic stroke (Benfenati et al., 2011; Donato et al., 2009; Kitchen et al., 2015; Vella et al., 2015). Under physiological conditions, AQP4 is highly polarized to astrocyte endfeet rather than non-endfeet processes and/or soma (Potokar et al., 2013). Our analysis reveals that AQP4 polarity is different between sham male and female mice, however, this finding was not consistent to both distal and proximal brain regions. Others have determined that estrogen increases AQP4 mRNA and protein quantities in adult mice (Shin et al., 2011). Following brain injury and ischemia, AQP4 expression is also increased (Fukuda and Badaut, 2012; Ribeiro Mde et al., 2006; Vella et al., 2015). Un-polarized AQP4 has been reported in proximity to the brain injury following more extended time points after stroke (Wang et al., 2012) and traumatic brain injury (Liu et al., 2015; Ren et al., 2013); a change in AQP4 polarity or absence of AQP4 impairs glymphatic clearance after injury (Iliff et al., 2014). Thus, we examined sex differences in AQP4 polarity (a distribution pattern) after 60 min MCA occlusion, rather than AQP4 quantity. Similar to others, we demonstrate that AQP4 is un-polarized in brain regions proximal to the ischemia induced by MCA occlusion in male mice. AQP4 also became un-polarized in female tissue, however, not as profoundly different as observations in male tissue. The lesser response noted in female proximal region is likely influenced by the normalization to sham, which was increased the female proximal region versus male. Therefore, our data best illustrate that the change from sham conditions was not as profound in female mice when compared to male. A change in AQP4 polarity just after 60 min of MCA occlusion is an indicator that AQP4 vesicle trafficking or insertion to the plasma membrane surface is disturbed due to cytotoxic events, cell swelling, and/or rearrangement of the cytoskeleton during gliosis (Potokar et al., 2013). Ensuring that AQP4 is correctly localized to endfeet is central to managing edema and ensuring efficient glymphatic clearance (Plog et al., 2015), both factors important to stroke recovery.

S100β is an astrocyte Ca^{2+} binding protein and small molecular messenger present in the astrocyte cytoplasm. Astrocytes release S100β in macro-molar concentrations after brain injury to act as a damage-associated molecular pattern (DAMP) molecule to promote inflammatory responses and affect astrocyte-microglia communication (Bianchi et al., 2010; Donato et al., 2009; Zhang et al., 2011). As such, S100β is of increasing interest as a

potential biomarker of brain injury and for its role in exacerbating inflammatory responses after stroke and traumatic brain injury (Dayon et al., 2011; Kiechle et al., 2014; Pham et al., 2010). The area of non-somatic S100β immunoreactivity was similar between male and female sham mice and therefore did not influence post-ischemia analysis. After ischemia, the area of non-somatic S100β is increased in males, with a lesser effect observed in female mice. In its role as a biomarker, Plog et al. (2015) provide evidence that S100β moves from brain parenchyma to the plasma via the glymphatic system and that the clearance of S100β to plasma is significantly impaired by un-polarized AQP4 distribution after traumatic brain injury or with the absence of AQP4 (APQ4-null mice). It will be vital to further clarify the role of sex differences in AQP4 polarity and glymphatic clearance of biomarkers such as S100β to the plasma. Such data is necessary to ensure the validity of interpreting peripheral concentrations of S100β as a biomarker of brain injury after stroke in males and females.

In conjunction with astrocytes, microglia cells have a robust and immediate response to injury. In a previous study we characterized the early microglia morphologic and functional response to 60 min MCA occlusion in male mice (Morrison and Filosa, 2013). We extend these findings and now show sex differences in microglia morphology immediately following MCA occlusion, however these changes are subtle. There was no sex differences in baseline microglia ramification observed in sham animals. However, following MCA occlusion, there were sex differences in the number of microglia process endpoints per cell and no sex differences in process length/cell. We also reveal evidence of sex differences in microglia function. Microglia CD11b is an integrin receptor key to microglia phagocytosis of endogenous structures and debris after ischemia (Kettenmann et al., 2011; Wake et al., 2009). We show that CD11b immunofluorescence is constitutively high in female sham tissue compared to males and remains unchanged after ischemic stroke whereas, in males, constitutively low levels of CD11b immunofluorescence is increased after brain ischemia. We suggest that elevated CD11b expression pattern prior to ischemia, observed in female mice, enhances microglia capacity to phagocytize necrotic debris and cell contents that may otherwise exacerbate neurotoxicity and neuronal death after stroke. Additional studies are necessary to clarify the benefits of early microglia phagocytosis to improve stroke outcomes.

We employ IHC methods in this study rather than other methods that quantify targeted antigens in tissue lysate; IHC is ideally suited to assess the location and distribution of targeted antigens. We and others have noted changes in AQP4 or S100β distribution, to become more diffuse, under experimental conditions or cell distribution (Dyck et al., 1993; Ren et al., 2013; Wang et al., 2012). However, IHC methods have inherent limitations and several factors must be considered when determining changes in AQP4 and S100β location and data interpretation (e.g. tissue integrity and associated diffusion of antibodies, unspecific immunodetection). To address this, we determined that there was negligible unspecific secondary immunoreactivity (for both astrocyte and microglia ICH protocols) in ipsilateral proximal tissue regions. In addition we provide evidence that after just 60 min of MCA occlusion (without reperfusion) cortical tissue integrity remians. We demonstrate that astrocytes remained active and viable and microglia volume was unchanged in the ipsilateral hemisphere after 60 min of MCA occlusion. In addition, using IHC, microglia morphology in the ipsilateral proximal tissue remained ramified and complex rather than amoeboid. Taken together, our observations support the notion that tissue integrity in cortical regions

imaged in this study were not severely compromised (as seen after ischemia and 24hr of reperfusion) so as to introduce unspecific biding during IHC protocols that would confound data analysis and interpretation. We also acknowledge that sex differences in brain infarct size in this mouse model of ischemic stroke has been previously shown after ischemia and 24hr of reperfusion, a conventional time point to measure infarct size due to the methodological constraints of 2,3,5-Triphenyltetrazolium chloride (TTC) staining (Banerjee et al., 2013; Bederson et al., 1986; Isayama et al., 1991; Liszczak et al., 1984; Shin et al., 2011). In this study, infarct size was not measured after 60 min of MCA occlusion because of the early time point and methodological constraints. Sex differences in ischemic injury at this early time-point post stroke may exist and therefore may be a source of variability we observe in our data analysis.

1.4 Conclusions

We present data of sex differences in astrocyte Ca^{2+} elevations as well as the astrocyte and microglia proteins known to have an important role in the evolution of brain injury after stroke. These findings are critical to contributions toward understanding sex differences not only in brain physiology but also stroke pathobiology. As we continue to elucidate origins of dichotomous stroke outcomes between the sexes, we move closer to the development of sex-specific and successful stroke therapies. Importantly, we address changes occurring at an early time point (prior to reperfusion) following ischemia with the goal to better understand and define the cellular targets involved in the evolution of ischemic stroke injury.

Acknowledgments

This study received financial support from NIHLB (R01HL089067) to JAF, NINR (1F32NR013611) to HWM

Abbreviations

Ca^{2+}	Calcium
MCA	Middle Cerebral Artery
AQP4	Aquaporin 4

References

Agulhon C, Sun MY, Murphy T, Myers T, Lauderdale K, Fiacco TA. Calcium Signaling and Gliotransmission in Normal vs. Reactive Astrocytes. Front Pharmacol. 2012; 3:139. [PubMed: 22811669]

Araque A, Parpura V, Sanzgiri RP, Haydon PG. Tripartite synapses: glia, the unacknowledged partner. Trends Neurosci. 1999; 22:208–215. [PubMed: 10322493]

Arganda-Carreras I, Fernandez-Gonzalez R, Munoz-Barrutia A, Ortiz-De-Solorzano C. 3D reconstruction of histological sections: Application to mammary gland tissue. Microsc Res Tech. 2010; 73:1019–1029. [PubMed: 20232465]

Attwell D, Buchan AM, Charpak S, Lauritzen M, Macvicar BA, Newman EA. Glial and neuronal control of brain blood flow. Nature. 2010; 468:232–243. [PubMed: 21068832]

Banerjee A, Wang J, Bodhankar S, Vandenbark AA, Murphy SJ, Offner H. Phenotypic Changes in Immune Cell Subsets Reflect Increased Infarct Volume in Male vs. Female Mice. Translational Stroke Research. 2013; 4:554–563. [PubMed: 24187596]

Bazargani N, Attwell D. Astrocyte calcium signaling: the third wave. Nat Neurosci. 2016; 19:182–189. [PubMed: 26814587]

Bederson JB, Pitts LH, Germano SM, Nishimura MC, Davis RL, Bartkowski HM. Evaluation of 2,3,5-triphenyltetrazolium chloride as a stain for detection and quantification of experimental cerebral infarction in rats. Stroke. 1986; 17:1304–1308. [PubMed: 2433817]

Benfenati V, Caprini M, Dovizio M, Mylonakou MN, Ferroni S, Ottersen OP, Amiry-Moghaddam M. An aquaporin-4/transient receptor potential vanilloid 4 (AQP4/TRPV4) complex is essential for cell-volume control in astrocytes. Proc Natl Acad Sci. 2011; 108:2563–2568. [PubMed: 21262839]

Bianchi R, Giambanco I, Donato R. S100B/RAGE-dependent activation of microglia via NF-kappaB and AP-1 Co-regulation of COX-2 expression by S100B, IL-1beta and TNF-alpha. Neurobiol Aging. 2010; 31:665–677. [PubMed: 18599158]

Brown GC, Neher JJ. Eaten alive! Cell death by primary phagocytosis: 'phagoptosis'. In Trends Biochem Sci. 2012; 37:325–332.

Chaban VV, Lakhter AJ, Micevych P. A membrane estrogen receptor mediates intracellular calcium release in astrocytes. Endocrinology. 2004; 145:3788–3795. [PubMed: 15131017]

Cheung G, Sibille J, Zapata J, Rouach N. Activity-Dependent Plasticity of Astroglial Potassium and Glutamate Clearance. Neural Plast. 2015; 2015:109106. [PubMed: 26346563]

Cordeau P Jr, Lalancette-Hebert M, Weng YC, Kriz J. Live imaging of neuroinflammation reveals sex and estrogen effects on astrocyte response to ischemic injury. Stroke. 2008; 39:935–942. [PubMed: 18258827]

Davalos D, Grutzendler J, Yang G, Kim JV, Zuo Y, Jung S, Littman DR, Dustin ML, Gan WB. ATP mediates rapid microglial response to local brain injury in vivo. In Nat Neurosci Vol. 2005; 8:752–758.

Dayon L, Turck N, Garci-Berrocoso T, Walter N, Burkhard PR, Vilalta A, Sahuquillo J, Montaner J, Sanchez JC. Brain extracellular fluid protein changes in acute stroke patients. J Proteome Res. 2011; 10:1043–1051. [PubMed: 21142207]

del Zoppo GJ. The neurovascular unit in the setting of stroke. J Intern Med. 2010; 267:156–171. [PubMed: 20175864]

Ding S, Wang T, Cui W, Haydon PG. Photothrombosis ischemia stimulates a sustained astrocytic Ca2+ signaling in vivo. Glia. 2009; 57:767–776. [PubMed: 18985731]

Dirnagl U, Iadecola C, Moskowitz MA. Pathobiology of ischaemic stroke: an integrated view. Trends in neurosciences. 1999; 22:391–397. [PubMed: 10441299]

Dirnagl U. Pathobiology of injury after stroke: the neurovascular unit and beyond. Ann N Y Acad Sci. 2012; 1268:21–25. [PubMed: 22994217]

Donato R, Sorci G, Riuzzi F, Arcuri C, Bianchi R, Brozzi F, Tubaro C, Giambanco I. S100B's double life: intracellular regulator and extracellular signal. Biochim Biophys Acta. 2009; 1793:1008–1022. [PubMed: 19110011]

Dyck RH, Van Eldik LJ, Cynader MS. Immunohistochemical localization of the S-100 beta protein in postnatal cat visual cortex: spatial and temporal patterns of expression in cortical and subcortical glia. Brain Res Dev Brain Res. 1993; 72:181–192. [PubMed: 8485842]

Filosa JA, Bonev AD, Nelson MT. Calcium dynamics in cortical astrocytes and arterioles during neurovascular coupling. In Circ Res. 2004; 95:e73–e81.

Filosa JA, Morrison HW, Iddings JA, Du W, Kim KJ. Beyond neurovascular coupling, role of astrocytes in the regulation of vascular tone. Neuroscience. 2015; 323:96–109. [PubMed: 25843438]

Franke H, Verkhratsky A, Burnstock G, Illes P. Pathophysiology of astroglial purinergic signalling. Purinergic Signal. 2012; 8:629–657. [PubMed: 22544529]

Fukuda AM, Badaut J. Aquaporin 4: a player in cerebral edema and neuroinflammation. J Neuroinflammation. 2012; 9:279. [PubMed: 23270503]

Gaberel T, Gakuba C, Goulay R, Martinez De Lizarrondo S, Hanouz JL, Emery E, Touze E, Vivien D, Gauberti M. Impaired glymphatic perfusion after strokes revealed by contrast-enhanced MRI: a new target for fibrinolysis? Stroke. 2014; 45:3092–3096. [PubMed: 25190438]

Gelderblom M, Leypoldt F, Steinbach K, Behrens D, Choe CU, Siler DA, Arumugam TV, Orthey E, Gerloff C, Tolosa E, Magnus T. Temporal and spatial dynamics of cerebral immune cell accumulation in stroke. Stroke. 2009; 40:1849–1857. [PubMed: 19265055]

Go AS, Mozaffarian D, Roger VL, Benjamin EJ, Berry JD, Blaha MJ, Dai S, Ford ES, Fox CS, Franco S, Fullerton HJ, Gillespie C, Hailpern SM, Heit JA, Howard VJ, Huffman MD, Judd SE, Kissela BM, Kittner SJ, Lackland DT, Lichtman JH, Lisabeth LD, Mackey RH, Magid DJ, Marcus GM, Marelli A, Matchar DB, McGuire DK, Mohler ER 3rd, Moy CS, Mussolino ME, Neumar RW, Nichol G, Pandey DK, Paynter NP, Reeves MJ, Sorlie PD, Stein J, Towfighi A, Turan TN, Virani SS, Wong ND, Woo D, Turner MB. Executive summary: heart disease and stroke statistics--2014 update: a report from the American Heart Association. Circulation. 2014; 129:399–410. [PubMed: 24446411]

Hansson E, Ronnback L. Glial neuronal signaling in the central nervous system. FASEB J Vol. 2003; 17:341–348.

Hinzman JM, DiNapoli VA, Mahoney EJ, Gerhardt GA, Hartings JA. Spreading depolarizations mediate excitotoxicity in the development of acute cortical lesions. Exp Neurol. 2015; 267:243–253. [PubMed: 25819105]

Hoyert DL, XJ. Deaths: Preliminary data for 2011. Vol. 61. Hyattsville, MD: National vital statistics reports National Center for Health Statistics; 2012. ed.^eds

Iliff JJ, Wang M, Zeppenfeld DM, Venkataraman A, Plog BA, Liao Y, Deane R, Nedergaard M. Cerebral arterial pulsation drives paravascular CSF-interstitial fluid exchange in the murine brain. J Neurosci. 2013; 33:18190–18199. [PubMed: 24227727]

Iliff JJ, Chen MJ, Plog BA, Zeppenfeld DM, Soltero M, Yang L, Singh I, Deane R, Nedergaard M. Impairment of glymphatic pathway function promotes tau pathology after traumatic brain injury. J Neurosci. 2014; 34:16180–16193. [PubMed: 25471560]

Isayama K, Pitts LH, Nishimura MC. Evaluation of 2,3,5-triphenyltetrazolium chloride staining to delineate rat brain infarcts. Stroke. 1991; 22:1394–1398. [PubMed: 1721247]

Iwabuchi S, Kawahara K. Oxygen-glucose deprivation-induced enhancement of extracellular ATP-P2Y purinoceptors signaling for the propagation of astrocytic calcium waves. Biosystems. 2009; 96:35–43. [PubMed: 19063934]

Kelly MJ, Ronnekleiv OK. Control of CNS neuronal excitability by estrogens via membrane-initiated signaling. Mol Cell Endocrinol. 2009; 308:17–25. [PubMed: 19549588]

Kettenmann H, Hanisch UK, Noda M, Verkhratsky A. Physiology of microglia. Physiol Rev. 2011; 91:461–553. [PubMed: 21527731]

Kiechle K, Bazarian JJ, Merchant-Borna K, Stoecklein V, Rozen E, Blyth B, Huang JH, Dayawansa S, Kanz K, Biberthaler P. Subject-specific increases in serum S-100B distinguish sports-related concussion from sports-related exertion. PLoS One. 2014; 9:e84977. [PubMed: 24416325]

Kim KJ, Iddings JA, Stern JE, Blanco VM, Croom D, Kirov SA, Filosa JA. Astrocyte contributions to flow/pressure-evoked parenchymal arteriole vasoconstriction. J Neurosci. 2015; 35:8245–8257. [PubMed: 26019339]

Kim WT, Rioult MG, Cornell-Bell AH. Glutamate-induced calcium signaling in astrocytes. Glia. 1994; 11:173–184. [PubMed: 7927645]

Kitchen P, Day RE, Taylor LH, Salman MM, Bill RM, Conner MT, Conner AC. Identification and Molecular Mechanisms of the Rapid Tonicity-induced Relocalization of the Aquaporin 4 Channel. J Biol Chem. 2015; 290:16873–16881. [PubMed: 26013827]

Kofuji P, Newman EA. Potassium buffering in the central nervous system. Neuroscience. 2004; 129:1045–1056. [PubMed: 15561419]

Kress BT, Iliff JJ, Xia M, Wang M, Wei HS, Zeppenfeld D, Xie L, Kang H, Xu Q, Liew JA, Plog BA, Ding F, Deane R, Nedergaard M. Impairment of paravascular clearance pathways in the aging brain. Ann Neurol. 2014; 76:845–861. [PubMed: 25204284]

Kuo J, Hamid N, Bondar G, Dewing P, Clarkson J, Micevych P. Sex differences in hypothalamic astrocyte response to estradiol stimulation. Biol Sex Differ. 2010; 1:7. [PubMed: 21208471]

Lawson LJ, Perry VH, Dri P, Gordon S. Heterogeneity in the distribution and morphology of microglia in the normal adult mouse brain. Neuroscience. 1990; 39:151–170. [PubMed: 2089275]

Lee Y, Lee SR, Choi SS, Yeo HG, Chang KT, Lee HJ. Therapeutically targeting neuroinflammation and microglia after acute ischemic stroke. Biomed Res Int. 2014; 2014:297241. [PubMed: 25089266]

Liszczak TM, Hedley-Whyte ET, Adams JF, Han DH, Kolluri VS, Vacanti FX, Heros RC, Zervas NT. Limitations of tetrazolium salts in delineating infarcted brain. Acta Neuropathol. 1984; 65:150–157. [PubMed: 6084391]

Liu H, Qiu G, Zhuo F, Yu W, Sun S, Li F, Yang M. Lost Polarization of Aquaporin4 and Dystroglycan in the Core Lesion after Traumatic Brain Injury Suggests Functional Divergence in Evolution. Biomed Res Int. 2015; 2015:471631. [PubMed: 26583111]

Liu W, Tang Y, Feng J. Cross talk between activation of microglia and astrocytes in pathological conditions in the central nervous system. Life Sci. 2011; 89:141–146. [PubMed: 21684291]

Madry C, Attwell D. Receptors, ion channels, and signaling mechanisms underlying microglial dynamics. J Biol Chem. 2015; 290:12443–12450. [PubMed: 25855789]

McCarthy MM, Arnold AP, Ball GF, Blaustein JD, De Vries GJ. Sex differences in the brain: the not so inconvenient truth. J Neurosci. 2012; 32:2241–2247. [PubMed: 22396398]

Miller VM, Kaplan JR, Schork NJ, Ouyang P, Berga SL, Wenger NK, Shaw LJ, Webb RC, Mallampalli M, Steiner M, Taylor DA, Merz CN, Reckelhoff JF. Strategies and methods to study sex differences in cardiovascular structure and function: a guide for basic scientists. Biol Sex Differ. 2011; 2:14. [PubMed: 22152231]

Morrison HW, Filosa JA. A quantitative spatiotemporal analysis of microglia morphology during ischemic stroke and reperfusion. J Neuroinflammation. 2013; 10:4. [PubMed: 23311642]

Mozaffarian D, Benjamin EJ, Go AS, Arnett DK, Blaha MJ, Cushman M, de Ferranti S, Despres JP, Fullerton HJ, Howard VJ, Huffman MD, Judd SE, Kissela BM, Lackland DT, Lichtman JH, Lisabeth LD, Liu S, Mackey RH, Matchar DB, McGuire DK, Mohler ER 3rd, Moy CS, Muntner P, Mussolino ME, Nasir K, Neumar RW, Nichol G, Palaniappan L, Pandey DK, Reeves MJ, Rodriguez CJ, Sorlie PD, Stein J, Towfighi A, Turan TN, Virani SS, Willey JZ, Woo D, Yeh RW, Turner MB. Heart disease and stroke statistics-2015 update: a report from the American Heart Association. Circulation. 2015; 131:e29–e322. [PubMed: 25520374]

Murphy, S.; Xu, J.; Kochanek, K. National vital statistics reports. Vol. 61. Hyattsville, MD: National Center for Health Statistics; 2013. Deaths: Final data for 2010. ed.^eds

Nedergaard M, Dirnagl U. Role of glial cells in cerebral ischemia. Glia. 2005; 50:281–286. [PubMed: 15846807]

Nedergaard M, Rodriguez JJ, Verkhratsky A. Glial calcium and diseases of the nervous system. In Cell Calcium. 2010; 47:140–149.

Pascual O, Ben Achour S, Rostaing P, Triller A, Bessis A. Microglia activation triggers astrocyte-mediated modulation of excitatory neurotransmission. In Proc Natl Acad Sci. 2012; 109:197–205.

Perego C, Fumagalli S, De Simoni MG. Temporal pattern of expression and colocalization of microglia/macrophage phenotype markers following brain ischemic injury in mice. J Neuroinflammation. 2011; 8:174. [PubMed: 22152337]

Pham N, Fazio V, Cucullo L, Teng Q, Biberthaler P, Bazarian JJ, Janigro D. Extracranial sources of S100B do not affect serum levels. PLoS One. 2010; 5

Plog BA, Dashnaw ML, Hitomi E, Peng W, Liao Y, Lou N, Deane R, Nedergaard M. Biomarkers of traumatic injury are transported from brain to blood via the glymphatic system. J Neurosci. 2015; 35:518–526. [PubMed: 25589747]

Potokar M, Stenovec M, Jorgacevski J, Holen T, Kreft M, Ottersen OP, Zorec R. Regulation of AQP4 surface expression via vesicle mobility in astrocytes. Glia. 2013; 61:917–928. [PubMed: 23505074]

Reeves MJ, Bushnell CD, Howard G, Gargano JW, Duncan PW, Lynch G, Khatiwoda A, Lisabeth L. Sex differences in stroke: epidemiology, clinical presentation, medical care, and outcomes. Lancet Neurol. 2008; 7:915–926. [PubMed: 18722812]

Ren Z, Iliff JJ, Yang L, Yang J, Chen X, Chen MJ, Giese RN, Wang B, Shi X, Nedergaard M. 'Hit & Run' model of closed-skull traumatic brain injury (TBI) reveals complex patterns of post-traumatic AQP4 dysregulation. J Cereb Blood Flow Metab. 2013; 33:834–845. [PubMed: 23443171]

Ribeiro Mde C, Hirt L, Bogousslavsky J, Regli L, Badaut J. Time course of aquaporin expression after transient focal cerebral ischemia in mice. J Neurosci Res. 2006; 83:1231–1240. [PubMed: 16511868]

Ritzel RM, Capozzi LA, McCullough LD. Sex, stroke, and inflammation: the potential for estrogen-mediated immunoprotection in stroke. Horm Behav. 2013; 63:238–253. [PubMed: 22561337]

Shin JA, Choi JH, Choi YH, Park EM. Conserved aquaporin 4 levels associated with reduction of brain edema are mediated by estrogen in the ischemic brain after experimental stroke. Biochim Biophys Acta. 2011; 1812:1154–1163. [PubMed: 21641993]

Srinivasan R, Huang BS, Venugopal S, Johnston AD, Chai H, Zeng H, Golshani P, Khakh BS. Ca(2+) signaling in astrocytes from Ip3r2(−/−) mice in brain slices and during startle responses in vivo. Nat Neurosci. 2015; 18:708–717. [PubMed: 25894291]

Takano, T.; Oberheim, N.; Cotrina, ML.; Nedergaard, M. In Stroke. Vol. 40. United States; 2009. Astrocytes and ischemic injury; p. S8-S12.ed.^eds

Thrane AS, Rappold PM, Fujita T, Torres A, Bekar LK, Takano T, Peng W, Wang F, Rangroo Thrane V, Enger R, Haj-Yasein NN, Skare O, Holen T, Klungland A, Ottersen OP, Nedergaard M, Nagelhus EA. Critical role of aquaporin-4 (AQP4) in astrocytic Ca2+ signaling events elicited by cerebral edema. Proc Natl Acad Sci. 2011; 108:846–851. [PubMed: 21187412]

Vella J, Zammit C, Di Giovanni G, Muscat R, Valentino M. The central role of aquaporins in the pathophysiology of ischemic stroke. Front Cell Neurosci. 2015; 9:108. [PubMed: 25904843]

Wake H, Moorhouse AJ, Jinno S, Kohsaka S, Nabekura J. Resting microglia directly monitor the functional state of synapses in vivo and determine the fate of ischemic terminals. In J Neurosci. 2009; 29:3974–3980.

Wang M, Iliff JJ, Liao Y, Chen MJ, Shinseki MS, Venkataraman A, Cheung J, Wang W, Nedergaard M. Cognitive deficits and delayed neuronal loss in a mouse model of multiple microinfarcts. J Neurosci. 2012; 32:17948–17960. [PubMed: 23238711]

Zhang L, Liu W, Alizadeh D, Zhao D, Farrukh O, Lin J, Badie SA, Badie B. S100B attenuates microglia activation in gliomas: possible role of STAT3 pathway. Glia. 2011; 59:486–498. [PubMed: 21264954]

Zheng W, Watts LT, Holstein DM, Prajapati SI, Keller C, Grass EH, Walter CA, Lechleiter JD. Purinergic receptor stimulation reduces cytotoxic edema and brain infarcts in mouse induced by photothrombosis by energizing glial mitochondria. PLoS One. 2010; 5:e14401. [PubMed: 21203502]

Zheng W, Talley Watts L, Holstein DM, Wewer J, Lechleiter JD. P2Y1R-initiated, IP3R-dependent stimulation of astrocyte mitochondrial metabolism reduces and partially reverses ischemic neuronal damage in mouse. J Cereb Blood Flow Metab. 2013; 33:600–611. [PubMed: 23321785]

Highlights

- Astrocyte Ca^{2+} dynamics are different in male and female mice after ischemia.
- Sex differences in astrocyte AQP4 polarity and non-somatic S100β after ischemia.
- Constitutive microglia CD11b is high in female sham cortex when compared to males.
- After ischemia, microglia CD11b immunoreactivity is not changed in female mice.
- Low baseline CD11b immunoreactivity is increased after ischemia in male mice.

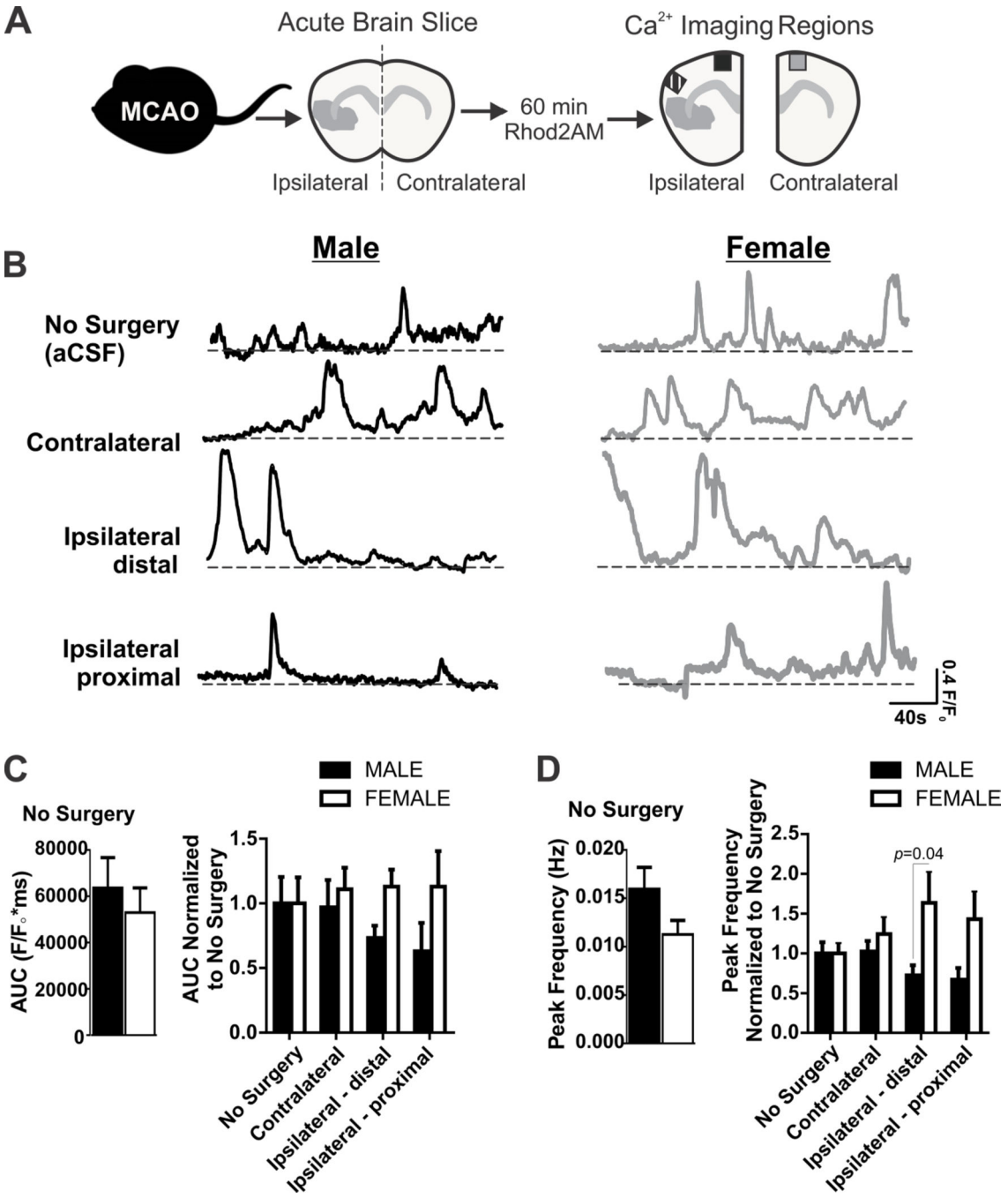

Figure 1. Astrocyte Ca^{2+} elevations in male and female mice after 60 min MCA occlusion

A) Experimental protocol for *ex vivo* Ca^{2+} imaging of acute brain slices after 60 min MCA occlusion. **B)** Representative Ca^{2+} traces acquired from male and female mice: no surgery (aCSF), contralateral, distal ipsilateral and proximal ipsilateral brain regions. **C)** Summary data of area under the curve (AUC) from Ca^{2+} traces acquired from spontaneously active astrocytes in male and female brain slices without surgery (left) and after 60 min MCA occlusion (right). N (male/female animals): No surgery (11/10), contralateral (16/11), distal ipsilateral (7/9); and proximal ipsilateral (5/11). AUC in male and female no surgery groups

(left, mean and SEM) are compared using unpaired Student's t-test: $p = 0.54$. Astrocyte Ca^{2+} AUC after 60min MCA occlusion (right), are compared using two-way ANOVA (mean and SEM): region: $p = 0.89$, sex: $p = 0.11$, interaction: $p = 0.68$. **D)** Summary data of Ca^{2+} peak frequency from spontaneously active astrocytes from male and female brain slices without surgery (left) and after 60 min MCA occlusion (right). N (male/female animals): No surgery (12/10), contralateral (16/12), distal ipsilateral (10/10); and proximal ipsilateral (8/11). Astrocyte Ca^{2+} peak frequency in male and female no surgery groups (left, mean and SEM) are compared using unpaired Student's t-test: $p = 0.11$. Peak frequency after 60min MCA occlusion (right) are compared using two-way ANOVA (mean and SEM): region: $p = 0.16$, sex: $p = 0.005$, interaction: $p = 0.16$ with Sidak multiple comparison analysis reported in figure.

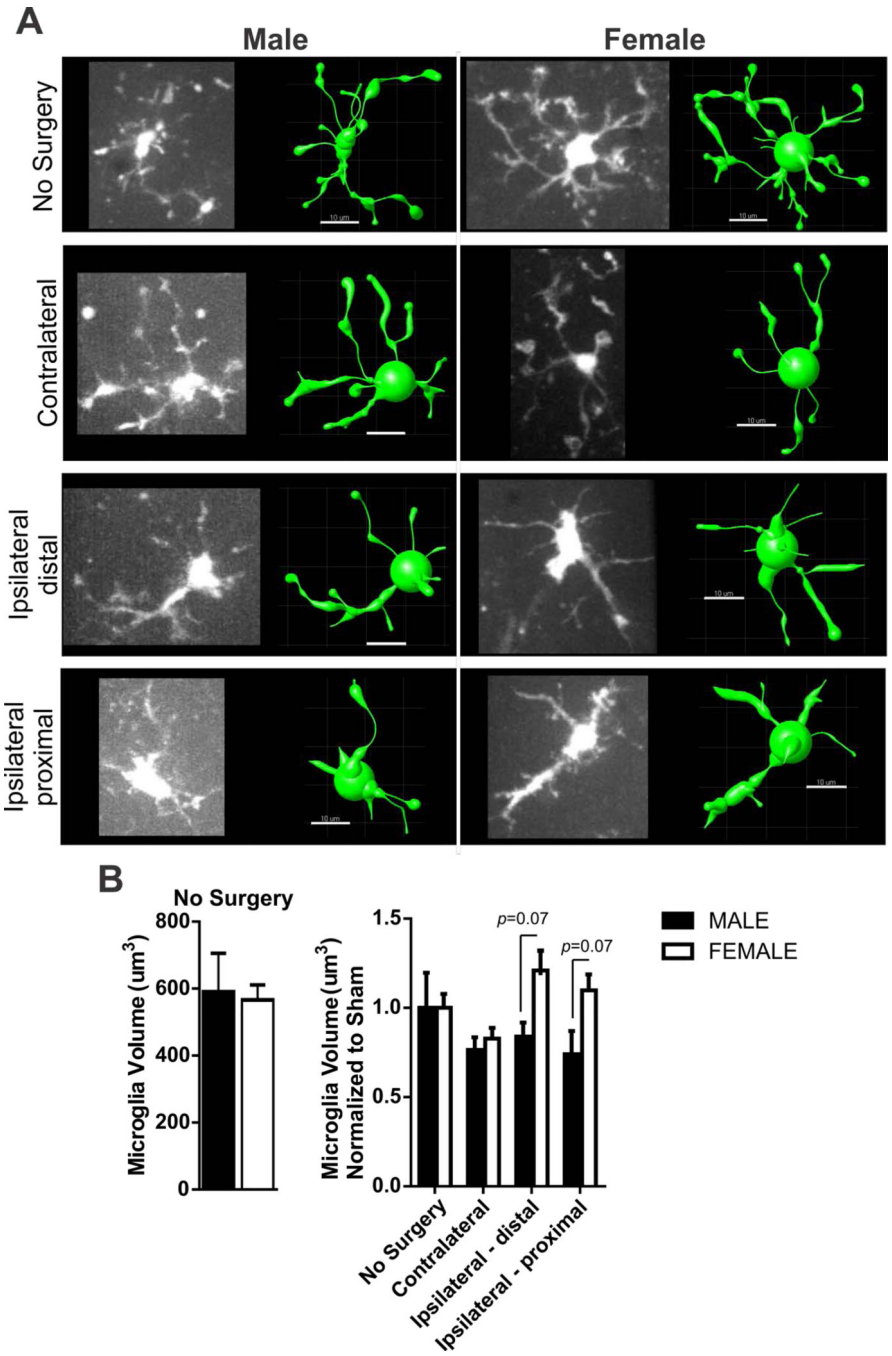

Figure 2. Sex differences in microglia volume after 60 min MCA occlusion

A) Example of microglia photomicrographs from *ex vivo* imaging (left) and rendered IMARIS model (right) after 60 min MCA occlusion according to group: no surgery, contralateral and ipsilateral brain regions. Scale bar = 10μm. **B)** Summary data of microglia volume in male and female brain slices without surgery (left) and after 60 min MCA occlusion (right). N (male/female animals): No surgery (4/5), contralateral (11/6), distal ipsilateral (6/4) proximal ipsilateral (5/8). Microglia volume in male and female no surgery groups (left, data and SEM) are compared using unpaired Student's t-test: $p = 0.84$.

Microglia volume (mean and SEM) after 60min MCA occlusion (right) is compared using two-way ANOVA: region, $p < 0.08$, sex, $p = 0.009$, interaction: $p = 0.17$ with Sidak multiple comparison analysis reported in figure.

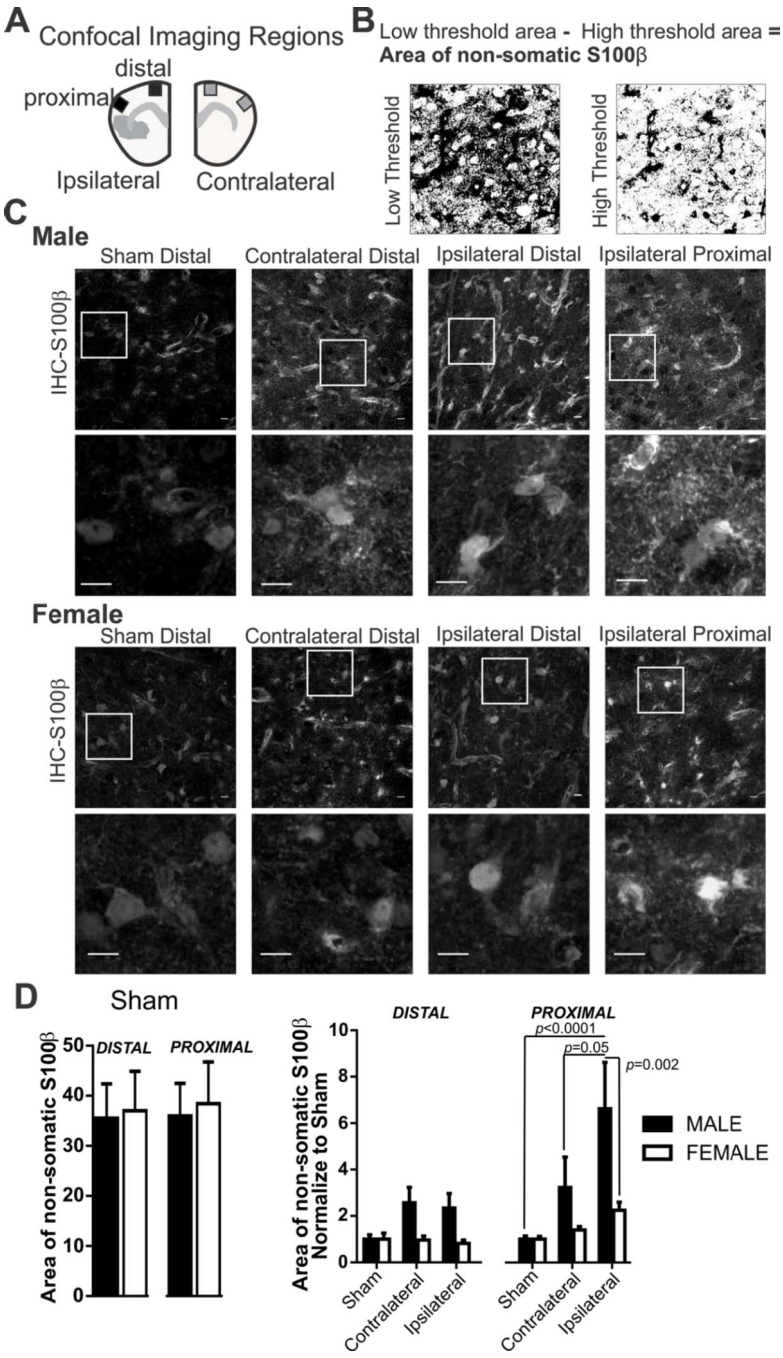

Figure 3. Sex differences in S100β expression pattern after 60 min MCA occlusion

A) Schematic drawing depicting regions imaged within cortical layers I–III in matching ipsilateral and contralateral brain sides with corresponding proximal and distal regions relative to the ischemic region. **B)** Example of high and low threshold binary images used to calculate non-somatic S100β. **C)** S100β immunostaining in male and female tissue after 60 MCA occlusion in sham, contralateral, and ipsilateral (distal and proximal) brain regions. Cropped photomicrographs corresponding to highlighted square shown in first row illustrate additional detail of somatic and non-somatic immunofluorescence. All data was collected

using full sized photomicrographs (Scale bars = 10μm). **D)** Summary data of non-somatic S100β after sham procedure (left) and after 60 min MCA occlusion (right) in male and female mice. N (male/female animals): Distal: Sham (9/6), contralateral (9/8), ipsilateral (9/8); Proximal: Sham (9/6), contralateral (9/8), ipsilateral (9/8). Non-somatic S100β in male and female sham mice (mean and SEM) are compared using an unpaired Student's t-test: distal $p = 0.89$; proximal, $p = 0.81$. Non-somatic S100β after 60min MCA occlusion in male and female mice (mean and SEM) are compared using two-way ANOVA: region, $p = 0.0007$, sex, $p = 0.0019$, interaction: $p = 0.12$ with Sidak multiple comparison analysis is reported in the figure.

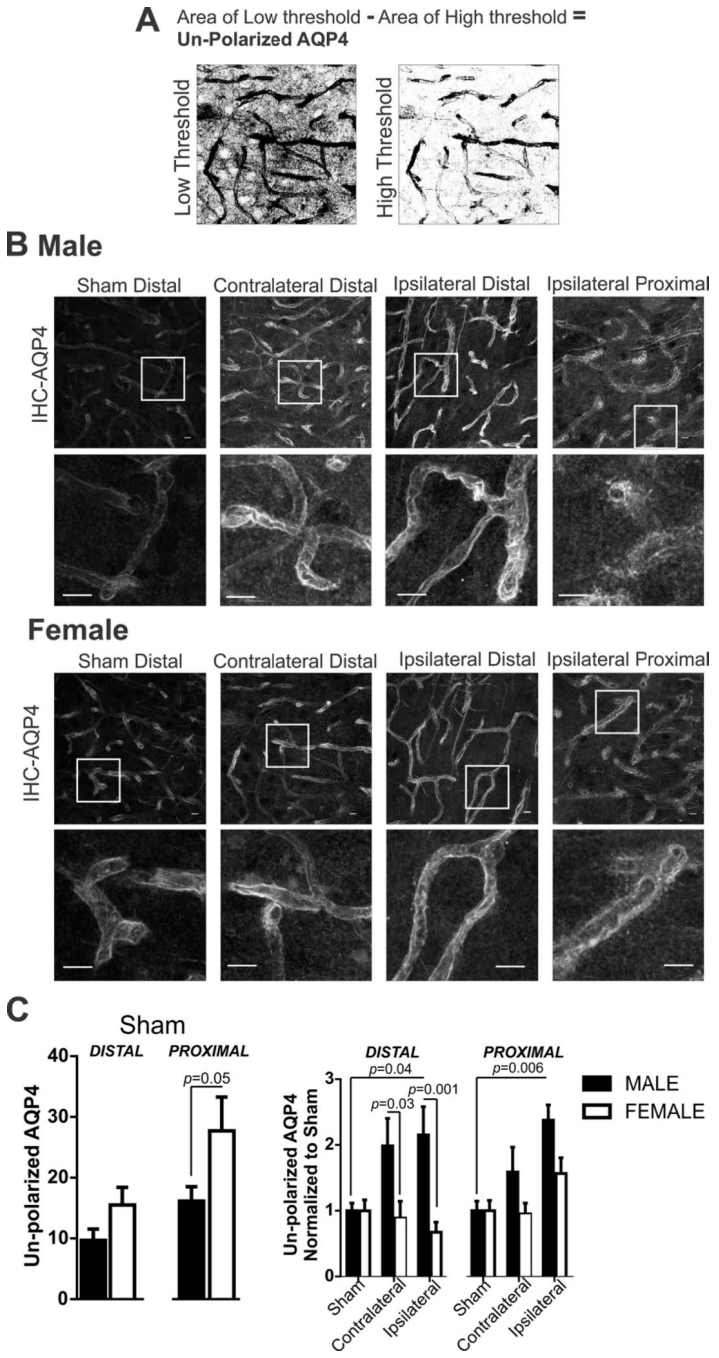

Figure 4. Sex differences in astrocyte AQP4 polarity after 60 min MCA occlusion

A) Example of high and low threshold binary images used to calculate AQP4 polarity. **B)** AQP4 immunostaining in male and female tissue after 60 min MCA occlusion in sham, contralateral, and ipsilateral brain regions. Cropped photomicrographs corresponding to highlighted squares shown in first row depicting additional details of polarized and un-polarized AQP4 expression pattern. All data was collected using full sized photomicrographs (Scale bars = 10μm). **C)** Summary data of AQP4 polarity after sham procedure (left) and after 60 min MCA occlusion in male and female mice. N (male/female animals): Distal:

Sham (9/6), contralateral (9/8), ipsilateral; Proximal: Sham (9/6), contralateral (9/8), ipsilateral. Un-polarized AQP4 in male and female sham mice (mean and SEM) are compared using an unpaired Student's t-test: distal, $p = 0.10$; proximal $p = 0.05$. Un-polarized AQP4 after MCA occlusion in male and female mice (mean and SEM) are compared using two-way ANOVA: region $p = 0.0089$, sex: $p < 0.0001$, interaction: $p = 0.064$. Sidak multiple comparison analysis is reported in the figure.

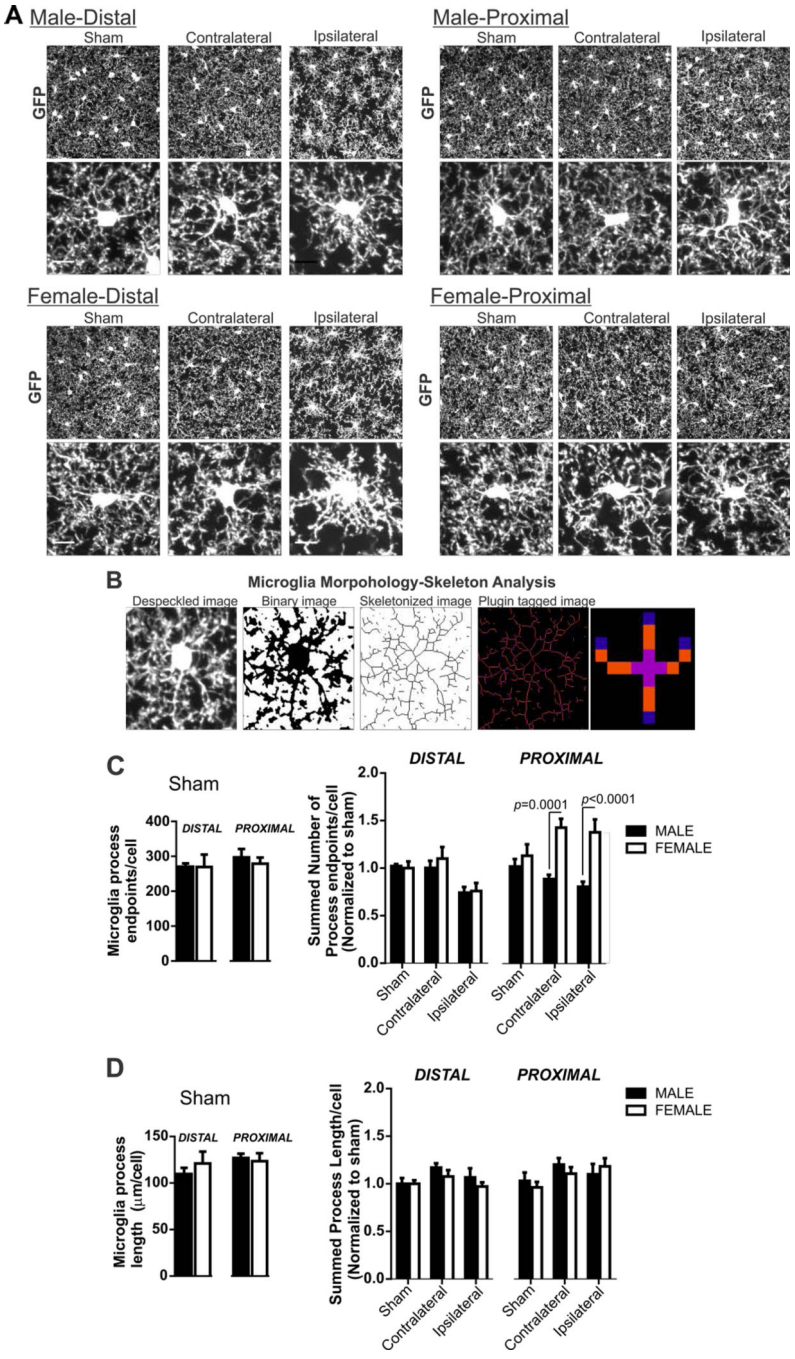

Figure 5. Microglia morphology in male and female mice after 60 min MCA occlusion

A) Microglia GFP immunostaining in male and female tissue after sham or 60 min MCA occlusion in contralateral, and ipsilateral distal and proximal brain regions. Cropped photomicrographs (below) show processes morphology details of an individual microglia. Analysis was completed on full sized photomicrographs (Scale bar = 10μm). **B)** Example of photomicrographs showing the computer-aided microglia morphology analysis method using ImageJ: photomicrographs are despeckled, converted to a binary image, skeletonized and then tagged using skeleton analysis plugin for data collection. The analyze skeleton

plugin identifies and tags skeletonized processes (orange) and endpoints (blue) http://imagejdocu.tudor.lu/doku.php?id=plugin:analysis:analyzeskeleton:start. **C)** Summary data of microglia process endpoints/cell after sham procedure (left) and after 60 min MCA occlusion in male and female mice: N (male/female animals): distal: sham (7/6), contralateral (9/9), ipsilateral (9/9); proximal: sham (7/6), contralateral (9/9), ipsilateral (9/9). Microglia endpoints/cell in male and female sham mice (mean and SEM) are compared using an unpaired Student's t-test: distal, $p = 0.44$; proximal $p = 0.74$. Process length/cell after MCA occlusion in male and female mice (mean and SEM) are compared using two-way ANOVA: region $p = 0.0001$, sex: $p < 0.0001$, interaction: $p = 0.0007$ with Sidak multiple comparison analysis is reported in figure. **D)** Summary data of microglia process length/cell after sham procedure (left) and after 60 min MCA occlusion in male and female mice. N (male/female animals): distal: sham (7/6), contralateral (9/9), ipsilateral (9/9); proximal: sham (7/6), contralateral (9/9), ipsilateral (9/9). Microglia process length/cell in male and female sham mice (mean and SEM) are compared using an unpaired Student's t-test: distal, $p = 0.98$; proximal $p = 0.57$. Process length/cell after MCA occlusion in male and female mice (mean and SEM) are compared using two-way ANOVA; region $p=0.10$, sex: $p<0.31$, interaction $p=0.78$.

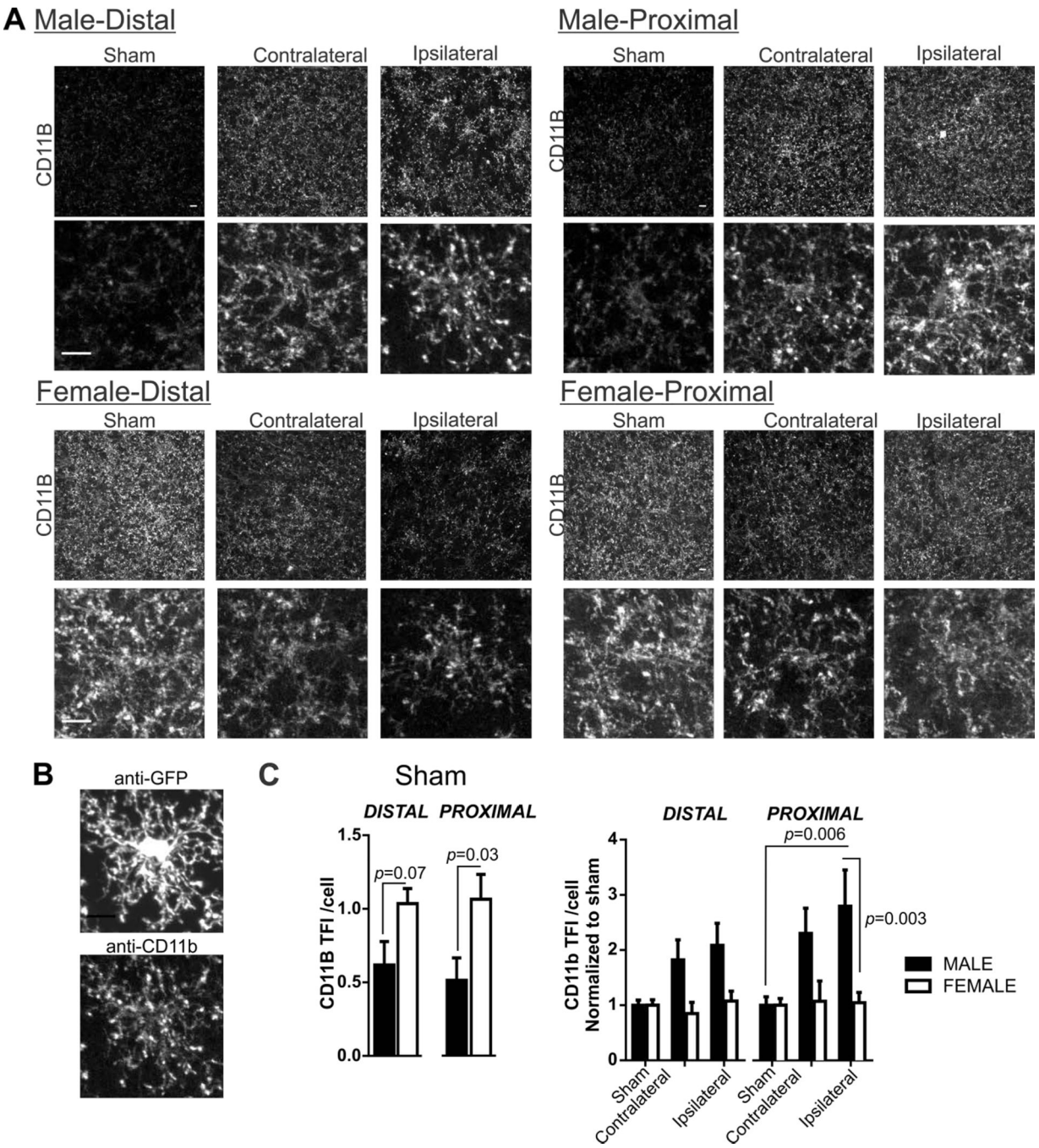

Figure 6. Microglia CD11b immunofluorescence in sham male and female mice and after 60 min MCA occlusion

A) Microglia CD11b immunostaining in male and female tissue after sham or 60 min MCA occlusion in contralateral, and ipsilateral distal and proximal brain regions. Bottom row, cropped photomicrographs showing details for an individual microglia CD11b distribution. **B**) GFP and CD11b immunostaining from a single microglia. **C)** Summary data of microglia CD11b after sham procedure (left) and after 60 min MCA occlusion in male and female mice. N (male/female animals): Distal: Sham (8/6), contralateral (9/8), ipsilateral (9/8);

Proximal: Sham (8/6), contralateral (9/8), ipsilateral (9/8). Summary data and analysis of microglia CD11b total fluorescence intensity (TFI)/cell in male and female sham tissue using Student's t-test: distal, $p = 0.07$; proximal, $p = 0.05$. Microglia CD11b TFI/cell after 60min MCA occlusion (mean and SEM) are compared using two-way ANOVA: region $p = 0.07$, sex: $p < 0.0001$, interaction: $p = 0.11$ with Sidak multiple comparison analysis is reported in figure.